CFD-FSI Analysis on Motion Control of Bio-Inspired Underwater AUV System Utilizing PID Control

Marvin Wright
Dept. of Naval Arcitecture Ocean and Marine Engineering
University of Strathclyde
Glasgow, United Kingdom
marvin.wright@strath.ac.uk

Yang Luo
Dept. of Naval Arcitecture Ocean and Marine Engineering
University of Strathclyde
Glasgow, United Kingdom
y.luo@strath.ac.uk

Qing Xiao
Dept. of Naval Arcitecture Ocean and Marine Engineering
University of Strathclyde
Glasgow, United Kingdom
qing.xiao@strath.ac.uk

Mark Post
Dept. of Electronic Engineering
University of York
York, United Kingdom
mark.post@york.ac.uk

Wael Gorma
Dept. of Electronic Engineering
University of York
York, United Kingdom
wael.gorma@york.ac.uk

Andrew Durrant
Dept. of R&D
PicSea Ltd.
Edinburgh, United Kingdom
andrew@picsea.co.uk

Hong Yue
Dept. of Electronic and Electrical Engineering
University of Strathclyde
Glasgow, United Kingdom
hong.yue@strath.ac.uk

Abstract— **For the design of a bio-inspired, fish-like robot with caudal fin, a Fluid Structure Interaction (FSI) analysis has been conducted to investigate the influence of material properties and undulation kinematics on hydrodynamic performance and efficiency. This supports the design process with focus on practical prototype build up.**

Keywords *CFD-FSI simulation, Bio-inspired AUV, Caudal fin, PID control*

I. INTRODUCTION AND LITERATURE REVIEW

Robots are an important tool in offshore windfarm Inspection Maintenance and Repair (IMR) operations extending human reach and providing safety. Autonomous Underwater Vehicles (AUV) with resident capabilities that mitigate recurring deployment times and costs are of high interest to industry [1]. In terms of operation capability, payload, and intervention time, a powerful AUV system is required to operate at high efficiency. Bio-inspired AUVs provide promising advantages over conventional torpedo and open-frame shaped designs in terms of efficiency, manoeuvrability, and modularity; however, they require additional design work with regard to kinematics and body design.

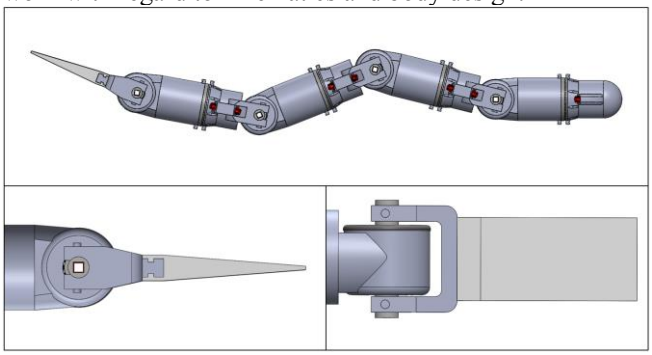

Figure 1 RoboFish - Windfarm inspection AUV showing caudal fin

As part of the EPSRC SuperGen ORE funded project "Autonomous Biomimetic Robot-fish for Offshore Wind Farm Inspection", a caudal fin was designed for a vertebrae structure bio-inspired AUV named "RoboFish". Directly attaching the caudal fin to an actuated joint facilitates active control, which makes it possible to optimize the interaction between the body and tail to enhance the propulsion performance. The detailed investigation of the caudal fin is motivated by the high importance to the overall design of manoeuvrability and thrust generation. In [1] Kelasidi et al. present significant thrust improvement and potential power savings provided by a passive caudal fin. The benefits of an actively controlled rigid caudal fin are also investigated in [2]. An experimental investigation of a rainbow trout inspired caudal fin actuated at the leading edge (LE) in pitch direction is published in [3].

By utilizing additive manufacturing techniques, we can manufacture a flexible caudal fin using a fused deposition method. In the literature, various types of soft materials have been used in underwater robots, for example, fluidic elastomer, ionic polymer-metal composite (IPMC), hydrogel, etc. [4][5]. However, a systematic analysis of the utilized materials on the propulsion performance is absent. Previous studies revealed that the material stiffness of the tail has an important effect on thrust production [6]. To help select the tail material for the prototype caudal fishtail, this work will explore the use of some soft materials popular in the robotic community to compare their performance in terms of thrust production and power expenditure. This provides an initial systematic analysis of the influence of material properties and actuation frequency on the hydrodynamic performance. The investigation is conducted using advanced numerical simulation techniques, showing feedback control of the fin's kinematics added to a strongly coupled fluid and structure solver.

Computational Fluid Dynamics (CFD) is a powerful tool used in the analysis of fluid flow problems. It provides unprecedented details in terms of flow visualization and

numerical data to enhance analysis capabilities for optimization in engineering designs. Coupled with a structural solver, it becomes a powerful analysis tool for flexible underwater structures. In this study, an in-house developed finite volume based CFD solver is coupled with the finite element-based structure solver CalculiX using the coupling library preCICE. FSI analysis is an efficient method of predicting the propulsion performance of a fishtail design with certain flexural rigidities. Added feedback control to the FSI simulations sheds light upon the required actuation parameters to achieve quasi-steady state swimming for detailed analysis at predicted swimming speeds. The closed-loop controller is set to adjust the generated thrust to equal the inlet velocity by adjusting the LE motion amplitude. The actuation parameters are directly related to the power consumption, which provide insight into the power requirement of the robotic fish.

II. Problem Description

Fish following Body-Caudal Fin (BCF) propulsion generate thrust by forming a travelling wave along their spinal cord. The muscle-imposed shape varies among species and is classified between Anguilliform (undulation) through to Thunniform (oscillation) as pictured in Figure 2.

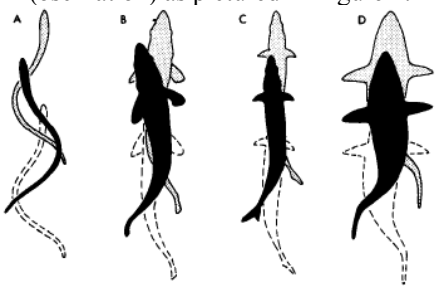

Figure 2 Swimming modes, A) Anguilliform, B) Subcarangiform, C) Carangiform, D) Thunniform [4]

The overall body propels by accelerating the surrounding fluid in opposite wave direction. This fluid acceleration is due to the pressure differences along the deforming body and reactive forces at the trailing edge (TE) of the swimmer as part of the vortex shedding. The body deformation of a robotic swimmer is induced via active motor control and can be optimized to increase efficiency. In search of high thrust efficacy, observations of natural swimmers suggest including a passive deforming body section at the tail in the form of a flexible caudal fin. The deformation of the fin is influenced by the forced motion at the LE together with the shape and rigidity of the fin interacting with the surrounding fluid domain.

For this numerical investigation, the setup is approximated as the quadrilateral 2D cross-section of a truncate caudal fin from the top view. It is noted that though in the present work, the considered geometry of the tail is two-dimensional, previous studies indicated that the effect patterns of stiffness on the propulsion performance are similar both in two- and three-dimensional models [7]. The setup and simulated perspective are detailed in Figure 3.

As shown in Figure 1, the LE of the fin is connected to an active joint of the robot; thus, it can be independently actuated, while the TE is set free and whose displacement is a result of the dynamic interplay of the tail and water. According to this setup, the LE will follow pitch motion according to equation 1:

$$\theta(t_s) = c_a\, A\, sin(2\pi\, f\, t_s) \tag{1}$$

Where θ is the LE pitch angle, A is the maximum angle of pitch, f is the frequency, t_s the time, and c_a is a controller output variable.

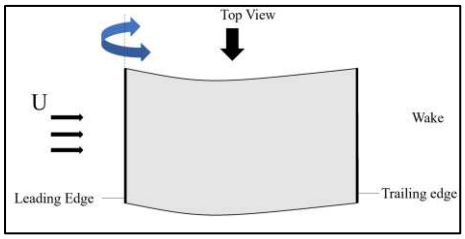

Figure 3 Simulation setup schematic showing top view on 2D cross

The dimensionless parameters governing this problem are defined as follows. The Reynolds number $Re = UL/\nu$, where L is the chord length of the fin, U the inlet velocity and ν the kinematic viscosity of water; the Strouhal number $St = f\, 2A_{TE}\,/U$ with A_{TE} the amplitude at TE; the reduced frequency $f^* = fL/U$; the mass ratio $m^* = \rho_s h/\rho_f L$ with ρ_s and ρ_f the density of the structure and fluid respectively and h is the thickness of the fin; the dimensionless stiffness $K = EI/\rho_s U^2 L^3$, where E is Young's modulus and $I = h^3/12$ is the area moment of inertia of the cross section.

A. Performance metrics

To gain insight into the hydrodynamic performance of different materials and their corresponding rigidities as well as how they operate at different frequencies, the analysis compares a matrix of the two. The matrix consists of three different materials, each at five different frequencies. Both the changing frequency and changing rigidity of the foil will lead to a different response.

The hydrodynamic performance is assessed using the thrust coefficient c_T,and power expenditure coefficient c_p defined as following:

$$c_T = -\frac{F_x}{\frac{1}{2}\,\rho_f U^2 L}, c_p = \frac{M_0\dot{\theta}}{\frac{1}{2}\,\rho_f U^2 L}, \tag{2}$$

where F_x is the horizontal force acting on the fin, M_0 is the angular momentum and $\dot{\theta}$ is the angular velocity of the rotation, both at the LE:

III. Methodology

The governing equations of the fluid surrounding the fin and the structural dynamics of the flapping fin are described. The fluid domain is represented by Ω_f with the boundary S_f. The structural domain is denoted by Ω_s with the boundary S_S. The fluid-structure interface is $S_i = S_f \cap S_S$ where the coupling is fulfilled. A pitch motion controller with feedback is applied to form a fluid-structure-control loop. The purpose is to adjust the pitch locomotion of the flexible fin to converge into a quasi-steady state during the dynamic interplay between the fluid and structure.

A. Governing equations and numerical approach

The flow around the fin is governed by the laws of conservation of mass, momentum and energy, which can be expressed in the integral form as

$$\frac{\partial}{\partial t}\iiint_{\Omega_f} \mathbf{U}\, d\Omega_f + \iint_{S_f} (\mathbf{F_c} - \mathbf{F_d})\, \mathbf{n} dS_f = 0, \quad (3)$$

where $\mathbf{U}$ is the conservative variable vector, $\mathbf{F_c}$ the convective flux, $\mathbf{F_d}$ the diffusion flux, and $\mathbf{n}$ denotes the normal unit vector in the outward direction.

The fluid domain is divided into a multi-block grid system with an array of hexahedral cells using a structured methodology. The fluid solver resolves viscous and compressible flow based on a cell-centred finite volume method. The central Jameson–Schmidt–Turkel scheme with an artificial dissipative term introduced by Jameson et al. [5] is applied to discretize the convective term. Green's theorem is used to obtain the first-order derivatives when calculating the viscous tensors. The dual-time stepping scheme is implemented for time integration for unsteady simulations [6]. Local time-stepping is implemented alongside the multigrid method to accelerate convergence. We also apply implicit residual smoothing to increase the stability of the solution. Employing Message Passing Interface (MPI) enables large-scale parallel computation within the programming environment of the fluid solver.

The governing law of the fin structure dynamics during flapping is the weak form of the balance of momentum, which can be written in the differential form as

$$\rho_s \frac{D^2\mathbf{W}}{D^2 t^2} = \nabla \mathbf{P} + \rho_s \mathbf{f}, \quad (4)$$

where the second derivatives of the displacement vector $\mathbf{W}$ yield the acceleration of the material point. The second Piola-Kirchoff stress tensor $\mathbf{P}$ denoting the surface forces and body forces per unit mass are presented by $\mathbf{f}$.

The finite element method is employed to discretize the governing equations. The utilization of the virtual work method enables us to obtain the linear algebraic equation system by discretizing the governing equation in the whole structural domain as

$$[\mathbf{K}]\{\mathbf{W}\} + [\mathbf{M}]\frac{D^2}{Dt^2}\{\mathbf{W}\} = \{\mathbf{F}\}, \quad (5)$$

where $[\mathbf{K}]$, $[\mathbf{M}]$ and $[\mathbf{F}]$ represent the global stiffness matrix, global mass matrix and global force vector, respectively. The temporal discretization is achieved by utilizing $\alpha-$ the method described in [7] with second-order accuracy. The structural solver is based on CalxuliX by Dhondt [7].

The coupling between the in-house fluid solver and structural solver is based on preCICE [8], a coupling library for partitioned multi-physics simulations. The interface quasi-Newton method with inverse Jacobian from a least-squares model (IQN-ILS) implemented in preCICE is used to stabilize the coupling and accelerate convergence. Communication between the fluid and structural solver is established via Transmission Control Protocol/Internet Protocol (TCP/IP) sockets. Radial basis function-based (RBF) interpolation is used to map the exchanged data between the two solvers. The details of the coupling framework and its validations are given in [9].

B. Feedback controller

While setting up the simulation, it is important to ensure different cases are compared at comparable conditions. To achieve this, all simulated fins are targeted to reach quasi-steady state, in other words, generate thrust force to balance the drag force at constant incoming velocity. Due to the characteristics of each case, the thrust generation varies; hence, the pitch amplitude to achieve a quasi-steady state must be found. This is achieved by implementing a feedback controller set to find a pitch amplitude to balance the cycle averaged drag and, as a consequence, the average force component in the velocity direction is zero. The feedback controller is coupled to the CFD FEA simulation environment by adding the controller output coefficient c_a to the displacement function in equation (1)

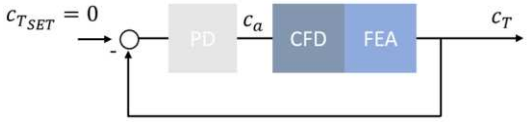

Figure 4 Feedback controller implementation schematic

The controller is implemented in the discrete incremental form with fixed sampling time. The sampling time is equal to the CFD time step. Equation (6) describes the controller output as a function of the error of the previous time step plus the incremental component of the current time step. Equation (7) shows the incremental calculation of the P and D component.

$$c_a(k) = c_a(k-1) + \Delta c_a(k) \quad (6)$$

$$\Delta c_a(k) = K_p[e(k) - e(k-1)] + \frac{K_d}{t_k\, t_s}[e(k) - 2e(k-1) + e(k-2)] \quad (7)$$

Here K_p and K_D are the tuning gains, k is the sample and t_k is a factor to equal K_d for all cases. The control error is set to be the time-averaged thrust coefficient:

$$e(k) = f\sum_{k=0}^{100} c_T(k)\, t_s \quad (8)$$

The tuned control gains for a close to critically damped system response are: $K_p = 5$ and $K_d = 0.2$.

C. Domain and case setup

All cases share the same simulation setup, except for variation of frequency and rigidity. The mesh domain of dimension 0.8m height by 2.1m width has the fin positioned horizontally with LE position at vertical centre and 0.5m from the left boundary, as pictured in Figure 5a. The left and right boundaries are assigned corresponding inlet and outlet conditions. Both horizontal boundaries are assigned far-field condition. The generated mesh contains 57424 cells and the minimum grid spacing is $1.67 \times 10^{-3}\, L$. Refinement is set towards the fin boundary to ensure correct calculation and capture of all physical effects, as pictured in Figure 5b. Mesh independency study can be found in [10]. The time step for each case is $t_s = T/100$.

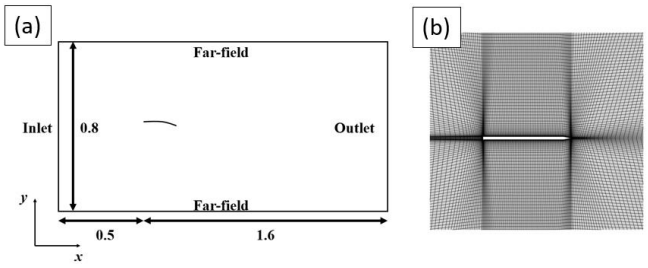

Figure 5 Domain setup and mesh refinement

The simulated geometry cross-section, pictured in Figure 5b, is inspired by the experimental investigation of [11]. To match the experimental setup, the Reynolds number equal for all cases is 6000 but assumed to be of laminar flow, and the mass ratio $m^* = 0.04$

For this investigation, the rigidity of the material is of uniform distribution, which reflects the targeted accessible adaptive manufacturing method. Three materials characterized by dimensionless stiffness are considered, in other words $K = 10$, $K = 1$ and $K = 0.25$. These correspond to a highly rigid material, a material of medium rigidity, and soft material. These will be called hard, medium and soft in the following. For all, the Poisson's ratio is 0.35.

For each material, the performance is assessed at 5 frequencies. Table 1 provides an overview of all simulated cases.

Table 1 Case overview

	$f^* = 0.75$	$f^* = 1$	$f^* = 1.5$	$f^* = 2$	$f^* = 2.5$
Soft	Case 1	Case 2	Case 3	Case 4	Case 5
Medium	Case 6	Case 7	Case 8	Case 9	Case 10
Hard	Case 11	Case 12	Case 13	Case 14	Case 15

IV. Controller Tuning and Stability

To examine the tracking performance of the controller, a tuning case summary is presented. Here, the controller gains are tuned manually following to the Ziegler-Nichols method. The PD controller gains have been found within 7 simulations.

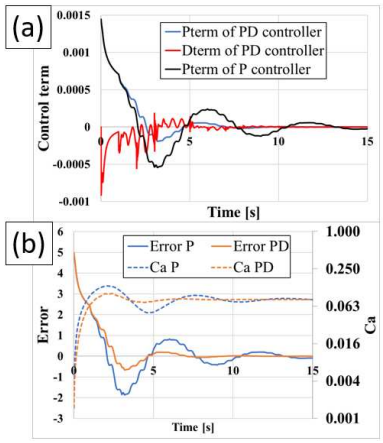

Figure 6 (a)Progression of error and controller output for P and PD controller. (b) P and PD term progression.

For the initial P controller, the output response c_a is stable yet overshoots with asymptotic convergence after around 15 oscillation periods. By adding a D gain the overshoot is damped and faster convergence is achieved after around 700 sampling periods. Figure 6(b) shows the dampening effect of the D-term reducing the overshoot of the P gain and achieving faster overall convergence. No steady-state error is observed; hence, there is no requirement to include an integral control.

V. Results and Analysis

Changes to the rigidity of the fin lead to differences in vertical displacement along the fin when excited at the same frequency. Generally, we observe that with the increase of frequency, the displacement of the TE decreases. It can be seen that at the same frequency, the more flexible the fin is, the larger the observed displacement. For a rigid fin, the observed TE amplitude changes little as the frequency is varied. With lower rigidities, the TE amplitude is more sensitive to frequency variation. However, for higher frequencies, the difference in TE amplitude between rigidities reduces to a minimum as seen in Figure 7(b). An analysis of the converged pitch angle for the medium fin shows a trend towards higher pitch amplitude for higher frequencies, while results for the soft fins show that the pitch amplitude reduces after an initial upward incline, Figure 7(c).

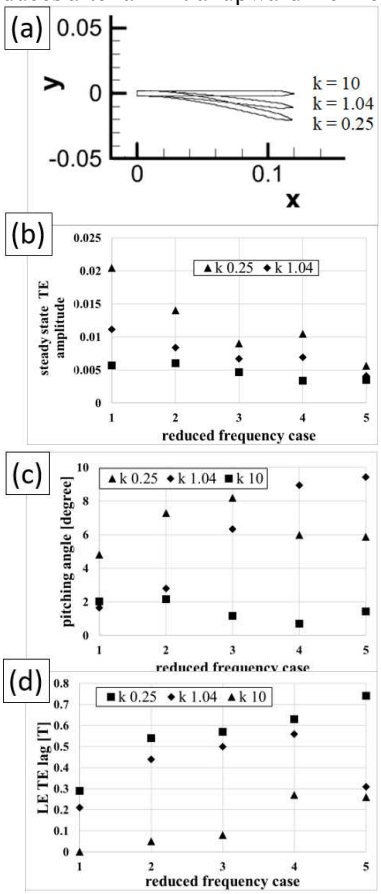

Figure 7 (a) Structure displacement at f=0.75, (b) TE amplitude, (c) QSS pitch amplitude (d) lag of TE behind pitch*

Figure 7(d) suggests that for increased pitch frequencies, the fin shape extends to show larger wave fractions. A more flexible structure leads to larger phase difference between LE and TE at the same frequency. From Figure 7(c), the results suggest increased thrust production of the soft fin at higher frequencies, while the medium fin requires higher pitch amplitudes for growing frequencies to provide thrust matching drag in order to yield quasi-steady state swimming.

The variation of the thrust coefficient within one oscillation period is depicted in Figure 8. The graph shows that the fin with medium flexibility has the maximum ability to entrain the surrounding flow to produce the largest thrust, although it also undergoes the largest drag. In comparison, the soft fin displays minimum force fluctuation where only negligible drag can be observed.

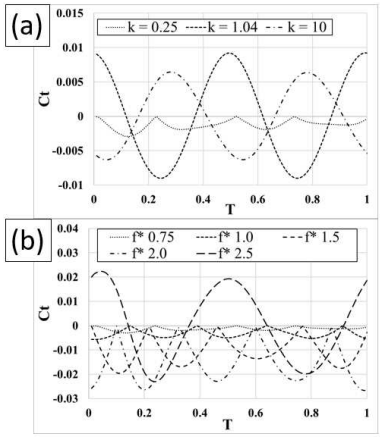

Figure 8 Instantaneous thrust coefficient (a) at f=0.75 and (b) k=0.25, both over one oscillation period T*

The instantaneous forces of the soft fin at converged pitch amplitude show a proportional increase in thrust force for growing frequency, Figure 9(a). However, a vertical shift between these can be observed.

In general, a higher frequency leads to a larger instantaneous thrust peak. In addition, an increased frequency also delays the occurrence of the peaks. The frequency indeed changes the achieved maximum values of thrust and drag forces, but these two peak values are almost equal for all the five cases, indicating the current PD controller works well to balance the unsteady drag and thrust to approach the desired quasi-steady state. Figure 9(b) shows the thrust coefficient amplitude envelope at the five frequencies for all rigidities

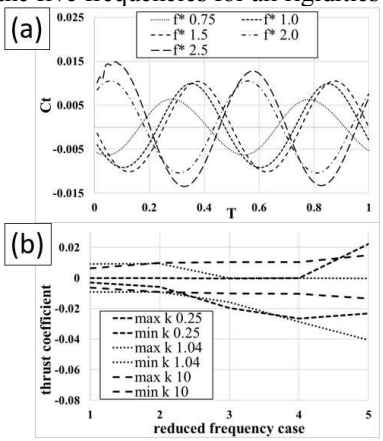

Figure 9 (a) Instantaneous thrust force of k 10 for all frequencies (b) Minimum and Maximum thrust boundaries for all k and frequencies., both over T.

Figure 10 shows the Z-vorticity of all 15 cases with cases of the same frequency sharing the same row. All rigidities show a trend to smaller vortexes for higher frequencies, which is in agreement with the reduced TE frequency in 8b. Furthermore, the phase lag between LE and TE leads to a difference in current shed vortex, seen for example, when comparing contours 1), 2) and 3). The contour also confirms the larger deflection of fins with lower rigidity. Figure 11 assesses two important design criteria for prototype build-up: controllability and power expenditure. For all cases, the same tuned control gains are used. Satisfactory convergence is observed for all cases after 50 oscillation periods. However, for a swimming prototype, fast convergence is desirable. Figure 11 a-c shows time progression of the controller output value c_a. Satisfying convergence is observed within 30 oscillation periods for all but one case. Differences in response from critically damped to limit cycle oscillation can be explained by the difference in error value magnitude of the individual joint.

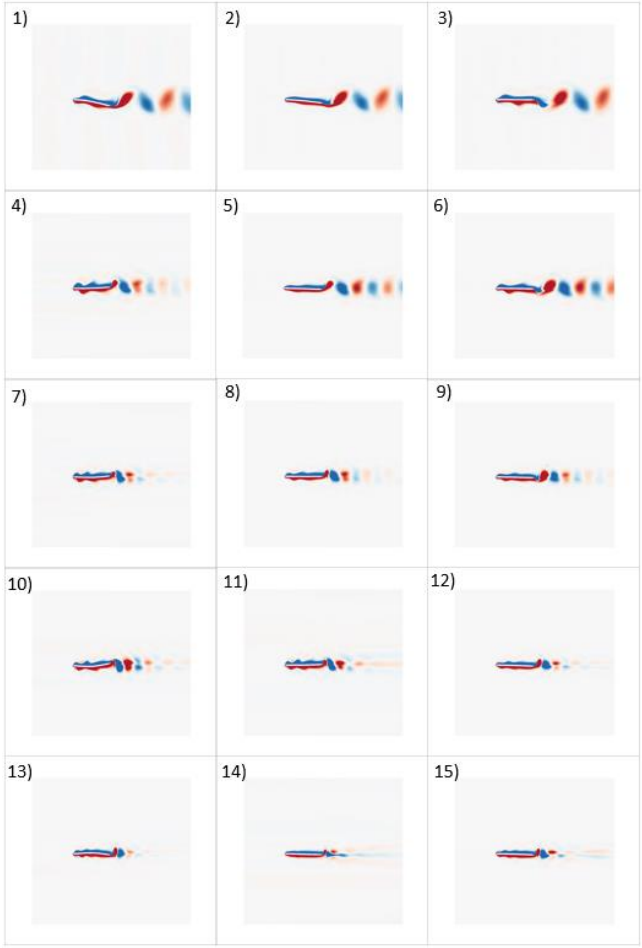

Figure 10 Z-vorticity contour at constant pitch amplitude at instant T for all 15 cases.

The power coefficient shown in Figure 11d generally follows the expectation that for higher frequencies the energy expenditure increases. While the power expenditure is similar for all materials at the first frequency, the medium stiffness displays energy advantages for frequency cases 2, 3 and 5.

Significant is also the drop in energy expenditure of the medium stiffness case 5, although the pitch amplitude is the highest of all cases. This could suggest improved efficiency of this case. Furthermore, the majority of lowest energy expenditures in conjunction with medium stiffness together with the good convergence over all frequencies suggests this is the optimal configuration of the three simulated.

The resulting Strouhal number for all cases, related to the freely moving TE, are close to the range of 0.2 – 0.4 observed in optimal fish swimming.

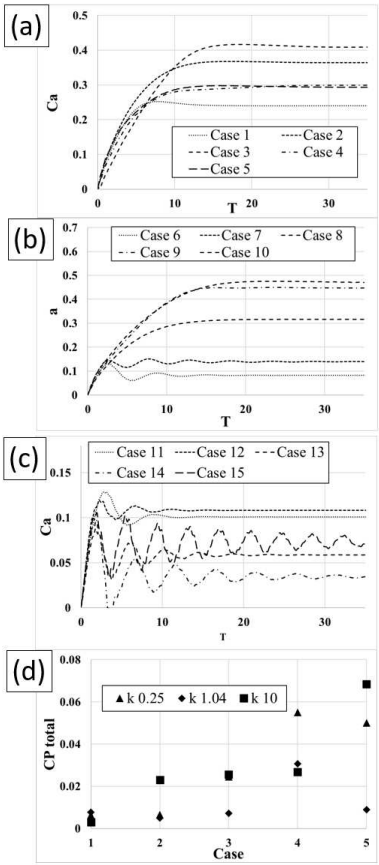

Figure 11 (a), (b), (c) progression of controller output variable a, (d) power expenditure coefficient

VI. Conclusion and Future Work

This work presents the numerical simulation of a flexible caudal fin crosssection at three different material properties and excited at 5 pitch frequencies at LE. The numerical simulation setup is complemented with a feedback controller to adjust the pitch amplitude to drive the drag component towards quasi-steady state. Results are presented in dimensionless values so they can be compared with the results of experimental investigations planned for the future. Results prove that all foils are able to generate sufficient thrust within the maximum pitch amplitude. For different material properties, changes in TE deflection and LE - TE phase are observed. Moreover, based on the results, the medium stiffness is considered the best of the three simulated. The investigation results provide the basis for design decisions and material selection in the build-up of a caudal fin.

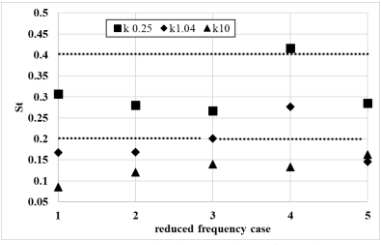

Figure 12 Strouhal number for all cases

Future work aims to extend the investigation to more material properties and swimming conditions. Furthermore, a comparison of numerical results and the built bio-inspired AUV prototype is planned.

VII. Acknowledgement

This research was made possible by an EPSRC Supergen ORE Hub Flexible Fund Program Grant "Autonomous Biomimetic Robot-fish for Offshore Wind Farm Inspection" EPSRC grant number EP/S000747/1. The Authors acknowledge the additional generous support provided by PicSea Ltd, East Coast Oil and Gas Engineering Ltd, and the UK Offshore Renewable Energy Catapult. The support of the White Rose Collaboration Fund is also acknowledged for bringing together expertise from the Universities of Leeds, Sheffield, and York that directly benefits this project and future AUVs.

References

[1] E. Kelasidi, A. M. Kohl, K. Y. Pettersen, B. Hoffmann, and J. T. Gravdahl, "Experimental investigation of locomotion efficiency and path-following for underwater snake robots with and without a caudal fin," *Annual Reviews in Control,* vol. 46, pp. 281-294, 2018.

[2] A. Gao and M. S. Triantafyllou, "Independent caudal fin actuation enables high energy extraction and control in two-dimensional fish-like group swimming," *Journal of Fluid Mechanics,* vol. 850, pp. 304-335, 2018.

[3] T. Salumäe and M. Kruusmaa, "A flexible fin with bio-inspired stiffness profile and geometry," *Journal of Bionic Engineering,* vol. 8, no. 4, pp. 418-428, 2011.

[4] W. Hoar and D. Randall, "Fish physiology. Locomotion, vol VII," ed: Academic Press, New York, 1978.

[5] A. Jameson, W. Schmidt, and E. Turkel, "Numerical solution of the Euler equations by finite volume methods using Runge Kutta time stepping schemes," in *14th fluid and plasma dynamics conference*, 1981, p. 1259.

[6] A. Jameson, "Time dependent calculations using multigrid, with applications to unsteady flows past airfoils and wings," in *10th Computational Fluid Dynamics Conference*, 1991, p. 1596.

[7] G. Dhondt, *The finite element method for three-dimensional thermomechanical applications*. John Wiley & Sons, 2004.

[8] H.-J. Bungartz *et al.*, "preCICE–a fully parallel library for multi-physics surface coupling," *Computers & Fluids,* vol. 141, pp. 250-258, 2016.

[9] Y. Luo, Q. Xiao, G. Shi, L. Wen, D. Chen, and G. Pan, "A fluid–structure interaction solver for the study on a passively deformed fish fin with non-uniformly distributed stiffness," *Journal of Fluids and Structures,* vol. 92, p. 102778, 2020.

[10] Y. Luo, Q. Xiao, and G. Shi, "A Fluid–Structure Interaction Study on a Bionic Fish Fin With Non-Uniform Stiffness Distribution," *Journal of Offshore Mechanics and Arctic Engineering,* vol. 142, no. 5, 2020.

[11] F. Paraz, C. Eloy, and L. Schouveiler, "Experimental study of the response of a flexible plate to a harmonic forcing in a flow," *Comptes Rendus Mécanique,* vol. 342, no. 9, pp. 532-538, 2014.